surfaces

Article

Evaluation of Photocatalytic Hydrogen Evolution in Zr-Doped TiO_2 Thin Films

Luis F. Garay-Rodríguez [1,*], M. R. Alfaro Cruz [1,2], Julio González-Ibarra [1], Leticia M. Torres-Martínez [1,3,*] and Jin Hyeok Kim [4]

1 Departamento de Ecomateriales y Energía, Facultad de Ingeniería Civil, Universidad Autónoma de Nuevo León, Cd. Universitaria, San Nicolás de los Garza 66455, Mexico; malfaroc@uanl.edu.mx (M.R.A.C.); julio.gonzalezibr@uanl.edu.mx (J.G.-I.)
2 Departamento de Ecomateriales y Energía, Facultad de Ingeniería Civil, CONAHCYT-Universidad Autónoma de Nuevo León, Cd. Universitaria, San Nicolás de los Garza 66455, Mexico
3 Centro de Investigación en Materiales Avanzados, S.C., Miguel de Cervantes 120 Complejo Industrial Chihuahua, Chihuahua 31110, Mexico
4 Department of Materials Science and Engineering and Optoelectronics Convergence Research Center, Chonnam National University, Yongbong-ro 77, Buk-gu, Gwangju 61186, Republic of Korea; jinhyeok@chonnam.ac.kr
* Correspondence: lgarayr@uanl.edu.mx or lfgarayr@gmail.com (L.F.G.-R.); lettorresg@yahoo.com or leticia.torres@uanl.edu.mx (L.M.T.-M.)

Abstract: Doping titanium dioxide has become a strategy for enhancing its properties and reducing its recombination issues, with the aim of increasing its efficiency in photocatalytic processes. In this context, this work studied its deposition over glass substrates using a sol–gel dip coating methodology. The effect of doping TiO_2 with Zirconium cations in low molar concentrations (0.01, 0.05, 0.1%) in terms of its structural and optical properties was evaluated. The structural characterization confirmed the formation of amorphous thin films with Zr introduced into the TiO_2 cell (confirmed by XPS characterization), in addition to increasing and defining the formed particles and their size slightly. These changes resulted in a decrease in the transmittance percentage and their energy band gap. Otherwise, their photocatalytic properties were evaluated in hydrogen production using ethanol as a sacrificial agent and UV irradiation. The hydrogen evolution increased as a function of the Zr doping, the sample with the largest Zr concentration (0.1% mol) being the most efficient, evolving 38.6 mmolcm^{-2} of this gas. Zr doping favored the formation of defects in TiO_2, being responsible for this enhancement in photoactivity.

Keywords: TiO_2; thin films; H_2 production; photocatalysis

Citation: Garay-Rodríguez, L.F.; Alfaro Cruz, M.R.; González-Ibarra, J.; Torres-Martínez, L.M.; Kim, J.H. Evaluation of Photocatalytic Hydrogen Evolution in Zr-Doped TiO_2 Thin Films. *Surfaces* **2024**, *7*, 560–570. https://doi.org/10.3390/surfaces7030038

Academic Editors: Irene Groot and Michalis Konsolakis

Received: 5 July 2024
Revised: 2 August 2024
Accepted: 6 August 2024
Published: 9 August 2024

1. Introduction

It is known that titanium dioxide as a photocatalyst has been widely used in different environmental applications mainly due to its chemical stability, low cost, and its adequate band position to perform simultaneous red-ox reactions [1]. On the other hand, some of its optical properties make it an ideal candidate to be used as a thin film [2]. In this context, using it as a thin film can maximize light absorption because of the maximization of the surface area used in the material [3]. Unfortunately, one of its most common issues is the fast recombination of photo-generated charges after its illumination. For this purpose, many strategies have been carried out to avoid or minimize this phenomenon, improving its physicochemical properties to enhance its reaction yields.

Metal doping has resulted as an efficient alternative to achieve these goals; moreover, in most cases, its band gap energy can be reduced so it can be activated in the visible-light region. Many reports have shown the effect of metal doping in photocatalytic processes, highlighting the use of some elements such as Cu- [4,5], Ag- [6,7], Au- [8,9], Pt- [10,11] Ni- [12,13], among others.

In this context, Zr is a good candidate for doping TiO_2 lattices because both elements are in the same group, have the same valence state, and the anatase phase supports Zr incorporation, forming the solid solution $Ti_{1-x}Zr_xO_2$ [14]. Some reports have studied the effect of Zr introduction into the TiO_2 anatase lattice on its physicochemical properties. For instance, Bolbol et al. [14] deposited Zr-doped TiO_2 thin films over glass substrates, varying the Zr dopant concentration from 0.5 to 10% mol using the sol–gel spin coating technique. They found changes in the structural and optical properties owing to a micro-strain increase created by Zr addition. This feature caused a reduction in electron–hole recombination compared to pristine TiO_2. Similarly, Juma et al. [15] and Oluwabi et al. [16] explored Zr-TiO_2 samples deposited by spray pyrolysis. In this context, Zr introduction in the TiO_2 lattice suppressed the anatase in the rutile phase transformation process, reduced the film roughness, decreased the film's crystallinity, and strongly increased the dielectric constant. In photocatalytic applications, Mbiri et al. [17] evaluated the Zr dopant content effect on TiO_2 thin films in the degradation of persistent organic pollutants, such as Chlorisazon, Phenol, and 4-Chlorophenol, finding a reduction in the recombination rate and achieving degradation percentages higher than 80%. Similar findings were reported by degrading formaldehyde [18], methylene blue [19–21], 4-Nitrophenol [22], bismark brown red [23], methylene orange [24], and 4-chlorophenol [25]. On the other hand, fewer reports have been observed in the case of hydrogen evolution; for instance, Chattopadhyay et al. [26]. prepared $Ti_{1-x}Zr_xO_{2-y}$ nanocrystals in different Zr compositions. They found that Zr^{4+} incorporation into the TiO_2 lattice modified the surface chemistry, caused lattice strain and increased the amount of Ti^{3+} species that favored the electron transference, reaching a superior hydrogen production compared with that of pristine TiO_2. Some other works have reported the effect of Zr dopant in TiO_2; however, most of them focus on the use of powder particles [27–30].

Considering the above, this work reports the findings of the effect of Zr doping on TiO_2 thin films deposited over a glass substrate by sol–gel dip coating in terms of their optical and structural properties. Also, the impact of these changes on the photocatalytic efficiency in the hydrogen evolution reaction using ethanol as sacrificial agent is described.

2. Materials and Methods

2.1. Thin Film Deposition

Pristine and Zr-doped TiO_2 thin films were deposited by the sol–gel chemical method. In this context, a Titanium butoxide (97% Sigma Aldrich, St. Louis, MO, USA) 3 M solution was prepared in isopropanol (DEQ), adding the appropriate %mol of Zirconium butoxide (97% Sigma Aldrich) to obtain 0.01, 0.05, or 0.1 mol of Zr in the media. All solutions were deposited over glass substrates (previously washed in separate isopropanol-acetone-water washings) using a dip coating technique. For this purpose, the glass substrates were placed vertically in the system and immersed three times into the solution at a constant speed. After each immersion cycle, the solvent was evaporated instantly by subjecting the substrates to a hot temperature (165 °C). Additionally, the films were calcined at 400 °C for 2 h to promote phase crystallization.

2.2. Characterization

The structural characterization of the films was evaluated using an X-ray PANanalytical diffractometer with Cu Ka 1.54 Å radiation at a grazing incidence angle. Surface images were taken in ASYLUM RESEARCH MFP3D-SA AFM equipment in tapping mode. Transmittance spectra were obtained with a UV–VIS/Cary 5000, running the samples at a 200–800 nm wavelength interval, and PL spectra were measured in an Agilent Cary Eclipse (excitation wavelength—325 nm) fluorescence spectrophotometer. XPS measurements were analyzed using a VG Multilab 2000 (Thermo VG Scientific equipment, Waltham, MA, USA) with a monochromatic MG-Kα (1253.6 eV) irradiation source.

2.3. Photocatalytic Reactions

Photocatalytic hydrogen production reactions were performed under UV (254 nm) irradiation using a cylindrical Pyrex batch reactor. Four films (30 cm^2 of active area) were pasted inside the reactor, adding 200 mL of deionized water. The system was vented with Argon for 15 min to promote an anoxic media, and then a UV lamp was immersed through a quartz tube and turned on. Gas samples were taken every 30 min using a syringe and injected in a gas chromatograph Varian GP-3380 with a thermal conductivity detector using Argon as the mobile phase and RESTEK REST-19808 (RESTEK, Centre County, PA, USA) column as a stationary phase. The acetaldehyde concentration in the remaining reaction liquid was measured by High-Resolution Liquid Chromatography using a Shimadzu Nexcol C18 (Shimadzu, Columbia, MD, USA) column as the stationary phase, and a mixture of acetonitrile/water 45:55 solution as the mobile phase.

3. Results and Discussion

Figure 1 presents the XRD patterns of all the samples. As seen, the pristine TiO_2 and the Zr-doped films were amorphous, and no diffraction peaks were detected. Similar results have been reported in the literature for TiO_2 films [31–34], where peaks with very low intensities or no peaks are detected in similar sol–gel deposition conditions.

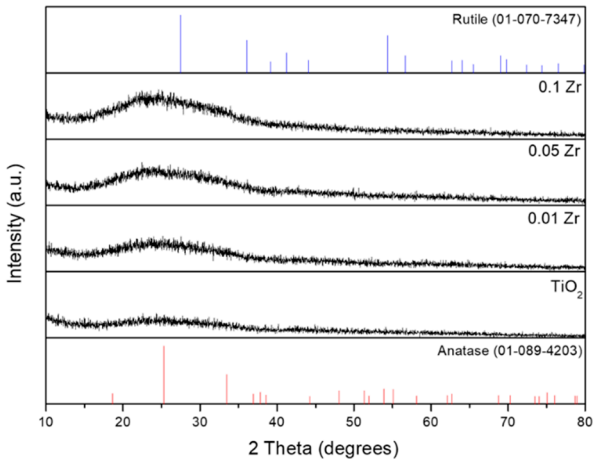

Figure 1. XRD patterns of the deposited Zr-doped TiO_2 thin films.

Figure 2 shows the elemental composition of the TiO_2 and Zr-doped TiO_2 films according to the XPS spectra for the C 1s, O 1s, Ti 2p, and Zr 3d levels. The C 1s core level has been deconvoluted into three peaks related to C-C, C-O-C, and O-C=O bonds (Figure 2a). On the other hand, the O1s spectra were deconvoluted into three curves for the TiO_2 and 0.01 Zr films and four curves for the 0.05 Zr and 0.1 Zr films. These curves correspond to the M-O, M-OH, C-OH, and C-O bonds [35,36], with only the 0.05 Zr and 0.1 Zr films showing the contribution of the C-OH species [35]. Due to the Zr being incorporated, the peak related to the M-O bond increased; likewise, the 0.01 Zr film is the only one that has less area in the peaks related to the M-OH and C-O bonds (Figure 2b).

Additionally, the Ti2p region is contributed to by the Ti^{3+}, Ti^{4+}, and $Ti(OH)_2$ (marked with *) species [36–38], while the Zr3d core level shows the presence of Zr^{4+} species [17,36]. In this context, the binding energy values obtained in the Zr 3d spectra are slightly lower to the ones reported in the ZrO_2 spectra, which suggests that the atoms are incorporated into the TiO_2 structure instead of in the ZrO_2 phase in low proportions [15]. Additionally, as the electronegativity of the Ti (1.54) is higher than that of the Zr (1.33), the peaks in the Ti2p and Zr3d spectra shifted toward a lower binding energy between the samples with Zr^{4+}, which is related to the partial substitution of Ti^{4+} by Zr^{4+} ions [15,36]. This feature can be related to the formation of a $Ti_{1-x}Zr_xO_2$ phase.

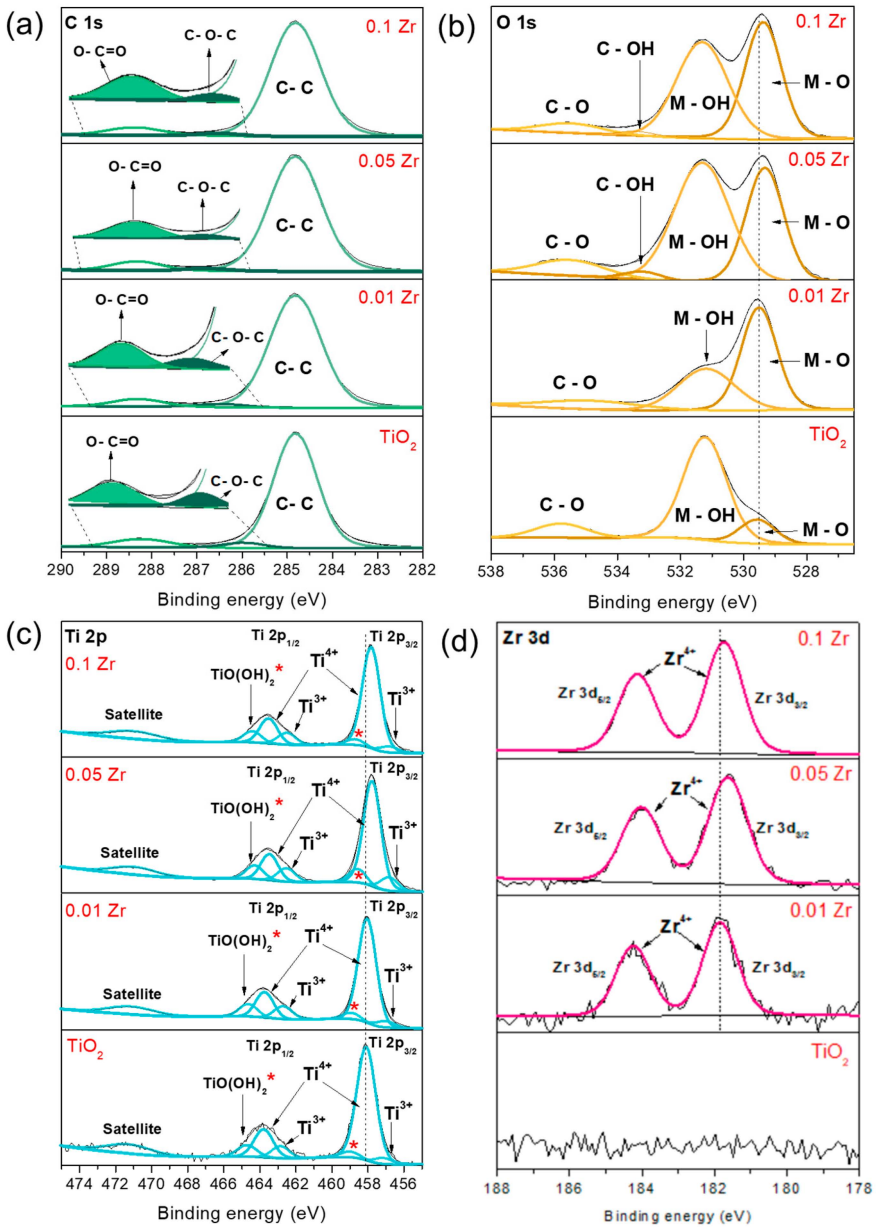

Figure 2. XPS core levels of (**a**) C 1s, (**b**) O 1s, (**c**) Ti 2p, and (**d**) Zr 3d.

Figure 3 presents the AFM images taken in a contact mode. As seen, all films were deposited uniformly; however, the pristine TiO_2 sample presented the formation of fine particles with the appearance of some cracks potentially generated during solvent evaporation. In contrast, the incorporation of Zr promoted the formation of densely packed particles, and additionally it reduced the formation of cracks, promoting a good coverage of the substrate. According to some authors, Zr incorporation as a dopant can retard the TiO_2 densification, reducing the formation of cracks and pinholes in the layer [39,40]. On the other hand, similarity can be seen between the TiO_2, 0.01 Zr, and 0.05 Zr samples; however, a slight reduction in the surface roughness was observed (Figure 3). Similar findings were reported by Naumenko et al. [39], where low Zr loads promoted the formation of densely packed particles as a result of the reduced crystallization effect that Zr promotes, or the increase in the nucleation centers during the film growth which inhibits grain growth, as Juma et al. mentions [15].

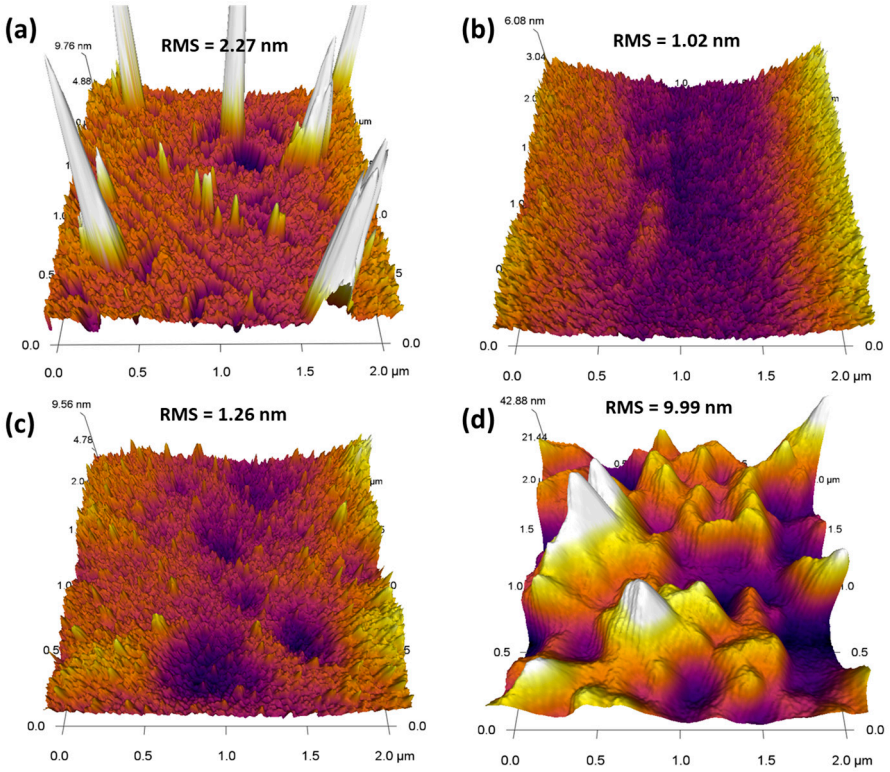

Figure 3. AFM characterization of the deposited films. (**a**) TiO_2; (**b**) 0.01 Zr; (**c**) 0.05 Zr; (**d**) 0.1 Zr.

On the contrary, a larger Zr concentration (0.1 Zr sample) promotes an increase in the film surface roughness; in this context, this drastic change can be associated with the formation of a more viscous sol due to the addition of a larger Zr precursor concentration [17]. An increase in the surface roughness can suggest an increase in the surface area, resulting in the presence of more active sites to enhance their photoactivity [41].

The transmittance percentage obtained from the deposited films is presented in Figure 4a. All the films are transparent in the visible light region (% T > 70%); however, when the Zr^{4+} concentration increases, the transmittance percentage slightly decreases, this behavior being related to high light dispersion over the film surface due to the increased roughness (more remarkable in the 0.1 Zr sample) [42,43]. The optical band gap of the films was calculated by the Tauc plot using the following equation [44]:

$$(\alpha h\nu) = A\left(h\nu - E_g\right)^n$$

where α is the absorption coefficient, $h\nu$ is the photon energy, A is a proportionality constant, n is the Tauc exponent ($n = 1/2$ for direct transitions and $n = 2$ for indirect transitions), and E_g is the band gap of the material [44,45]. Figure 4b shows a Tauc plot, where the band gap values slightly decrease with the incorporation of Zr (TiO_2 = 3.88 eV; 0.01 Zr = 3.81 eV; 0.05 Zr = 3.85 eV; 0.1 Zr = 3.76 eV). This decrease in the band gap value is related to shifts in the absorption edge toward a higher wavelength, which is due to an increase in the doping carrier concentrations. These carriers interact with free carriers and ionized impurities, causing a decrease in the band gap value [46]. In our films, as the Zr^{4+} concentration increases, the absorption edge shifts to higher wavelengths, decreasing the band gap value due to the increase in different impurities from the Zr^{4+}. According to Bolbol et al., this phenomenon is known as the Burstein–Moss effect [14].

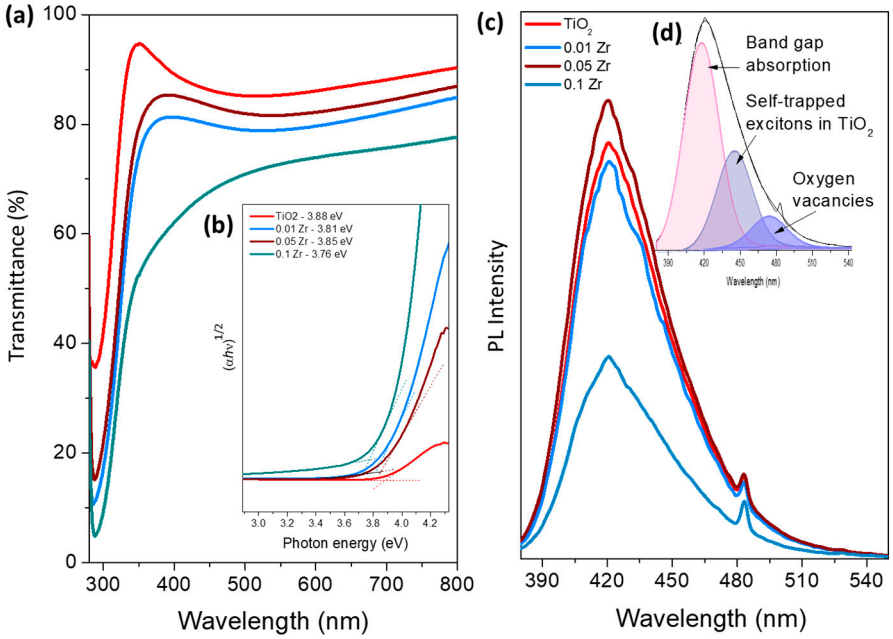

Figure 4. Optical properties as (**a**) transmittance percentage, (**b**) band gap (Tauc plot), (**c**) PL spectra, and (**d**) PL spectrum deconvoluted from the TiO_2 and Zr-doped TiO_2 films.

The PL spectra of the films excited with a wavelength of 320 nm are shown in Figure 4c. As seen, all the samples presented a broad emission between 390 and 540 nm. As this band displays a broad emission, this region could be deconvoluted into three bands, which are related to the TiO_2 band gap absorption (∼420 nm), self-trapped excitons in TiO_2 (∼450 nm), and oxygen vacancies of TiO_2 and of ZrO_2 and Zr^{4+} (∼430 to 530 nm) [47–49] (Figure 4d). On the other hand, from Figure 4c, there is an evident decrease in the PL intensity in the samples with a larger load of Zr^{4+}; in this context, it is well known that the PL emission reduction is associated with a minimization of the e^-/h^+ recombination, which translates into a greater availability of free charges to carry out red-ox reactions [50]. Additionally, it is known that the doping process produces extra free electrons in the TiO_2 lattice, which also reduces the emission efficiency by creating a non-radiative channel [14].

The photocatalytic hydrogen evolution rates obtained from the deposited films using ethanol as a sacrificial agent are presented in Figure 5a. As seen, all the samples present photoactivity, which is enhanced because of the increase in the Zr^{4+} concentration, reaching almost double the TiO_2 production (22 $mmolcm^{-2}$) in the sample loaded with 0.1%mol of Zr (38.6 $mmolcm^{-2}$). In this context, this observed improvement in the photocatalytic activity can be related to different facts; for instance, a larger Zr concentration causes a greater roughness on the film surface, which, as mentioned previously, increases the surface area and the active sites where ethanol molecules can be adsorbed and react to produce hydrogen. Additionally, the 0.1 Zr sample presented reduced electron–hole recombination, evidenced by the PL analyses, mainly associated with the formation of energy levels below the TiO_2 conduction band as self-trapped excitons, and defects such as oxygen vacancies.

Figure 5b presents the possible mechanism of hydrogen production through ethanol oxidation. In this context, the use of this organic compound has been highlighted by its capacity to act as an electron donor to the conduction band, enhancing the hydrogen production compared with using pure water [29]. Additionally, the presence of the different defects can capture light-induced electrons; for instance, in the case of oxygen vacancies, they play an important role acting as electron (e^-) traps, which, in consequence, avoid their recombination with the holes (h^+) [51]. Moreover, Zr^{4+} doping also introduces alternative defect levels close to the conduction band of TiO_2, which also can act as electron trap centers because the presence of Zr metal is used to produce a Schottky barrier to facilitate electron capture [52].

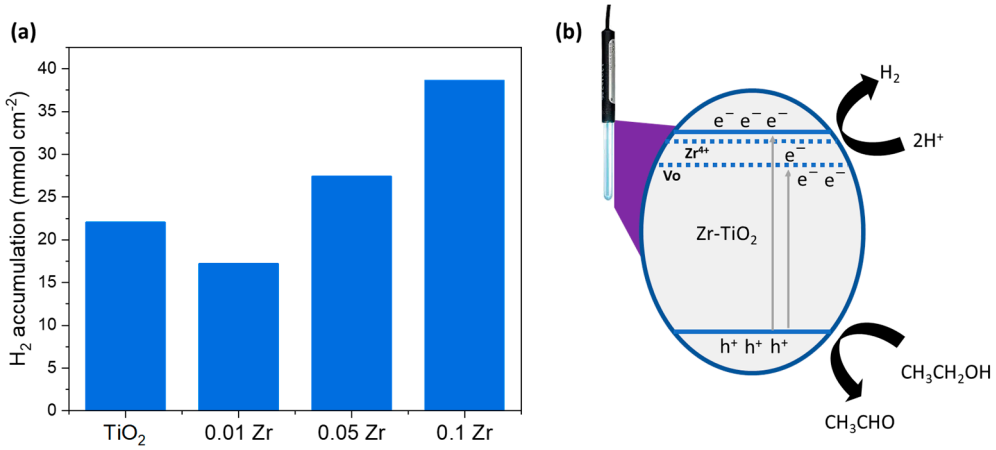

Figure 5. (**a**) Photocatalytic hydrogen production rate as function of the surface area. (**b**) Proposed mechanism of the hydrogen evolution using Zr-doped TiO_2.

On the other hand, ethanol is oxidated in the Zr-TiO_2 film valence band, forming acetaldehyde. The formation of this compound was evidenced in the remaining liquid of the reaction, detecting the following concentrations: TiO_2 = 750 µmol, 0.01 Zr = 627 µmol, 0.05 Zr = 612 µmol, 0.1 Zr = 530 µmol. Finally, the protons (H^+) formed from ethanol oxidation react with the electrons (e^-) accumulated in the formed defects and the conduction band to efficiently produce hydrogen.

Finally, Table 1 presents a summary of the hydrogen evolution reaction via photocatalysis or photo-electrocatalysis using TiO_2 thin films deposited under different methodologies. In this context, some studies focus on analyzing the different deposition conditions related to the used methodology, while others analyze the effect of an added dopant concentration (added in situ or as a multi-layer). As seen, the hydrogen production values obtained in this work are comparable with those that present higher production values, which suggests that doping TiO_2 with this metal (Zr) is an alternative to enhance its photocatalytic performance.

Table 1. Summary of the photocatalytic hydrogen production studies using TiO_2 thin films.

Photocatalyst	Dopant	Deposition Method	Illumination	Sacrificial Agent	Hydrogen Production	Ref.
TiO_2	Cu-Ni	Drop casting	300 W Xe lamp	Methanol 25%	41,690 µmol/gh	[53]
TiO_2	--	DC sputtering	UV 254 nm lamp	--	38 µmol	[54]
TiO_2	--	Hydrothermal	UV 254 nm lamp	--	132 µmol	[55]
TiO_2	--	RF sputtering	300 W Xe lamp	--	0.55 µmol/hcm^2	[56]
TiO_2	Au-Pd	Spin coating	300 W Xe lamp	Glycerol 5%	0.014 mL/min	[57]
TiO_2	Ag	Sol–gel/dip coating	5000 W Xe lamp	KOH 1 M	580 µmol	[58]
TiO_2	Ag	Drop casting	420 W Hg lamp	Water/methanol 1:1	148 µmol/gh	[59]
TiO_2	Cr	RF sputtering	250 W W lamp	NaOH 1 M	24 µmol/h	[60]
TiO_2	Ag	Hydrothermal	16 W Hg lamp	Ethanol 10%	8.1 µmol/cm^2	[61]
TiO_2	Pt	Dip coating	Black light lamps	Ethanol 50%	9 µmol/min	[62]
TiO_2	Pt	RF sputtering Sol–gel/spin coating	250 W W lamp	NaOH 1M	12.5 µmol/h 4.3 µmol/h	[63]
TiO_2	N-NiO N-CuO	Sol–gel/dip coating	UV 254 nm lamp	--	62,000 µmol/g	[64]
TiO_2	Pt	Dip coating	13 W UV lamp	Water/methanol 1:1	349.6 µmol/gh	[65]
TiO_2	Zr	Anodization method	500 W Xe lamp	Artificial sea water/ethilenglycol	15 µmol	[30]
TiO_2	Zr	Sol–gel/dip coating	UV 254 lamp	ethanol	38,600 µmol/cm^2	This work

4. Conclusions

Zr-doped TiO_2 amorphous thin films were successfully grown over glass substrates using the sol–gel dip coating methodology, varying the Zr concentration in the film precursor solution (0.01, 0.05 and 0.1 mol%). The incorporation of Zr^{4+} into the TiO_2 cell was confirmed using XPS, which resulted in the possible formation of the $Ti_{1-x}Zr_xO_2$ phase. The increase in the Zr concentration caused changes in the structural and optical properties of the films such as an increase in the film roughness, and a slight reduction in the transmittance percentage and their band gap. All the films exhibited photoactivity, evolving hydrogen under UV irradiation and ethanol as a sacrificial agent, with the hydrogen accumulation being increased by almost double in the samples with the largest Zr load (0.1 Zr = 38.6 mmolcm^{-2}) compared with that of pristine TiO_2 film. This enhancement in the photocatalytic activity was associated with the increase in the roughness of these films, which resulted in an increased surface area and was favorable for the reaction, and with the formation of different defects near to the TiO_2 conduction band that acted as electron trap centers and minimized the e^-/h^+ recombination rate.

Author Contributions: L.F.G.-R. and M.R.A.C.: conceptualization, methodology, investigation, data curation, writing—original draft. J.G.-I.: methodology, data curation. L.M.T.-M.: resources, supervision, writing—review and editing. J.H.K.: resources, supervision. All authors have read and agreed to the published version of the manuscript.

Funding: This research was founded by Consejo Nacional de Humanidades, Ciencias y Tecnologías: 320379; Universidad Autónoma de Nuevo León: PAICYT 275-CE-2022; PAICYT 277-CE-2022; National Research Foundation of Korea: 2022R1A2C2007219.

Institutional Review Board Statement: Not applicable.

Informed Consent Statement: Not applicable.

Data Availability Statement: The data that support the findings of this study are available from the corresponding author upon reasonable request.

Acknowledgments: The authors express their gratitude to the Centro de Investigación en Materiales Avanzados (CIMAV), specially Luz Ibarra and Oscar Vega for their valuable assistance with the AFM characterization, and to the Chonnam National University for the XPS measurement. Julio González thanks CONAHCYT for his 1148572 "Ayudante de Investigador" grant.

Conflicts of Interest: The authors declare no conflicts of interest.

References

1. Pant, B.; Park, M.; Park, S.-J. Recent Advances in TiO_2 Films Prepared by Sol-Gel Methods for Photocatalytic Degradation of Organic Pollutants and Antibacterial Activities. *Coatings* **2019**, *9*, 613. [CrossRef]
2. Alam, M.J.; Cameron, D.C. Preparation and Characterization of TiO_2 Thin Films by Sol-Gel Method. *J. Solgel Sci. Technol.* **2002**, *25*, 137–145. [CrossRef]
3. Nalajala, N.; Patra, K.K.; Bharad, P.A.; Gopinath, C.S. Why the Thin Film Form of a Photocatalyst Is Better than the Particulate Form for Direct Solar-to-Hydrogen Conversion: A Poor Man's Approach. *RSC Adv.* **2019**, *9*, 6094–6100. [CrossRef] [PubMed]
4. Liu, L.; Gao, F.; Zhao, H.; Li, Y. Tailoring Cu Valence and Oxygen Vacancy in Cu/TiO_2catalysts for Enhanced CO_2photoreduction Efficiency. *Appl. Catal. B* **2013**, *134–135*, 349–358. [CrossRef]
5. Colón, G.; Maicu, M.; Hidalgo, M.C.; Navío, J.A. Cu-Doped TiO_2 Systems with Improved Photocatalytic Activity. *Appl. Catal. B* **2006**, *67*, 41–51. [CrossRef]
6. Zhao, C.; Krall, A.; Zhao, H.; Zhang, Q.; Li, Y. Ultrasonic Spray Pyrolysis Synthesis of Ag/TiO_2 Nanocomposite Photocatalysts for Simultaneous H_2 Production and CO_2 Reduction. *Int. J. Hydrogen Energy* **2012**, *37*, 9967–9976. [CrossRef]
7. Li, H.; Wu, X.; Wang, J.; Gao, Y.; Li, L.; Shih, K. Enhanced Activity of AgMgOTiO_2 Catalyst for Photocatalytic Conversion of CO_2 and H_2O into CH_4. *Int. J. Hydrogen Energy* **2016**, *41*, 8479–8488. [CrossRef]
8. Puga, A.V.; Forneli, A.; García, H.; Corma, A. Production of H_2 by Ethanol Photoreforming on Au/TiO_2. *Adv. Funct. Mater.* **2014**, *24*, 241–248. [CrossRef]
9. Khatun, F.; Abd Aziz, A.; Sim, L.C.; Monir, M.U. Plasmonic Enhanced Au Decorated TiO_2 Nanotube Arrays as a Visible Light Active Catalyst towards Photocatalytic CO_2 Conversion to CH_4. *J. Environ. Chem. Eng.* **2019**, *7*, 103233. [CrossRef]
10. Galin, A.; Walendziewski, J. Photocatalytic Water Splitting over Pt-TiO_2 in the Presence of Sacrificial Reagents. *Energy Fuels* **2005**, *19*, 1143–1147.

11. Xiong, Z.; Wang, H.; Xu, N.; Li, H.; Fang, B.; Zhao, Y.; Zhang, J.; Zheng, C. Photocatalytic Reduction of CO_2 on Pt^{2+}-Pt0/TiO_2 Nanoparticles under UV/Vis Light Irradiation: A Combination of Pt^{2+} Doping and Pt Nanoparticles Deposition. *Int. J. Hydrogen Energy* **2015**, *40*, 10049–10062. [CrossRef]
12. Luna, A.L.; Dragoe, D.; Wang, K.; Beaunier, P.; Kowalska, E.; Ohtani, B.; Bahena Uribe, D.; Valenzuela, M.A.; Remita, H.; Colbeau-Justin, C. Photocatalytic Hydrogen Evolution Using Ni-Pd/TiO_2: Correlation of Light Absorption, Charge-Carrier Dynamics, and Quantum Efficiency. *J. Phys. Chem. C* **2017**, *121*, 14302–14311. [CrossRef]
13. Ong, W.-J.; Gui, M.M.; Chai, S.-P.; Mohamed, A.R. Direct Growth of Carbon Nanotubes on Ni/TiO_2 as next Generation Catalysts for Photoreduction of CO_2 to Methane by Water under Visible Light Irradiation. *RSC Adv.* **2013**, *3*, 4505. [CrossRef]
14. Bolbol, A.M.; Abd-Elkader, O.H.; Elshimy, H.; Zaki, Z.I.; Shata, S.A.; Kamel, M.; Radwan, A.S.; Mostafa, N.Y. The Effect of Zr (IV) Doping on TiO_2 Thin Film Structure and Optical Characteristics. *Results Phys.* **2022**, *42*, 105955. [CrossRef]
15. Juma, A.; Oja Acik, I.; Oluwabi, A.T.; Mere, A.; Mikli, V.; Danilson, M.; Krunks, M. Zirconium Doped TiO_2 Thin Films Deposited by Chemical Spray Pyrolysis. *Appl. Surf. Sci.* **2016**, *387*, 539–545. [CrossRef]
16. Oluwabi, A.T.; Juma, A.O.; Oja Acik, I.; Mere, A.; Krunks, M. Effect of Zr Doping on the Structural and Electrical Properties of Spray Deposited TiO_2 Thin Films. *Proc. Est. Acad. Sci.* **2018**, *67*, 147. [CrossRef]
17. Mbiri, A.; Taffa, D.H.; Gatebe, E.; Wark, M. Zirconium Doped Mesoporous TiO_2 Multilayer Thin Films: Influence of the Zirconium Content on the Photodegradation of Organic Pollutants. *Catal. Today* **2019**, *328*, 71–78. [CrossRef]
18. Taechasirivichai, K.; Chiarakorn, S.; Chawengkijwanich, C.; Pongprayoon, T.; Chuangchote, S. Ceramic Tiles Coated with Zr-Ag Co-doped TiO_2 Thin Film for Indoor Air Purifying and Antimicrobial Applications. *Int. J. Appl. Ceram. Technol.* **2022**, *20*, 2019–2029. [CrossRef]
19. Song, J.; Wang, X.; Yan, J.; Yu, J.; Sun, G.; Ding, B. Soft Zr-Doped TiO_2 Nanofibrous Membranes with Enhanced Photocatalytic Activity for Water Purification. *Sci. Rep.* **2017**, *7*, 1636. [CrossRef]
20. Schiller, R.; Weiss, C.K.; Landfester, K. Phase Stability and Photocatalytic Activity of Zr-Doped Anatase Synthesized in Miniemulsion. *Nanotechnology* **2010**, *21*, 405603. [CrossRef]
21. Bathula, C.; Nissimagoudar, A.S.; Kumar, S.; Jana, A.; Sekar, S.; Lee, S.; Kim, H.-S. Enhanced Photodegradation of Methylene Blue by Zr-Doped TiO_2:A Combined DFT and Experimental Investigation. *Inorg. Chem. Commun.* **2024**, *164*, 112442. [CrossRef]
22. Wang, C.; Geng, A.; Guo, Y.; Jiang, S.; Qu, X.; Li, L. A Novel Preparation of Three-Dimensionally Ordered Macroporous M/Ti (M=Zr or Ta) Mixed Oxide Nanoparticles with Enhanced Photocatalytic Activity. *J. Colloid Interface Sci.* **2006**, *301*, 236–247. [CrossRef] [PubMed]
23. Divya, G.; Jaishree, G.; Sivarao, T.; Lakshmi, K.V.D. Microwave Assisted Sol–Gel Approach for Zr Doped TiO_2 as a Benign Photocatalyst for Bismark Brown Red Dye Pollutant. *RSC Adv.* **2023**, *13*, 8692–8705. [CrossRef]
24. Liao, X.; Ren, H.-T.; Shen, B.; Lin, J.-H.; Lou, C.-W.; Li, T.-T. Enhancing Mechanical and Photocatalytic Properties by Surface Microstructure Regulation of TiO_2 Nanofiber Membranes. *Chemosphere* **2023**, *313*, 137195. [CrossRef] [PubMed]
25. Lukáč, J.; Klementová, M.; Bezdička, P.; Bakardjieva, S.; Šubrt, J.; Szatmáry, L.; Bastl, Z.; Jirkovský, J. Influence of Zr as TiO_2 Doping Ion on Photocatalytic Degradation of 4-Chlorophenol. *Appl. Catal. B* **2007**, *74*, 83–91. [CrossRef]
26. Chattopadhyay, S.; Mondal, S.; De, G. Hierarchical $Ti_{1-x}Zr_xO_{2-y}$ Nanocrystals with Exposed High Energy Facets Showing Co-Catalyst Free Solar Light Driven Water Splitting and Improved Light to Energy Conversion Efficiency. *J. Mater. Chem. A Mater.* **2017**, *5*, 17341–17351. [CrossRef]
27. Pahi, S.; Sahu, S.; Singh, S.K.; Behera, A.; Patel, R.K. Visible Light Active Zr- and N-Doped TiO_2 Coupled g-C_3N_4 Heterojunction Nanosheets as a Photocatalyst for the Degradation of Bromoxynil and Rh B along with the H_2 Evolution Process. *Nanoscale Adv.* **2021**, *3*, 6468–6481. [CrossRef]
28. Barba-Nieto, I.; Caudillo-Flores, U.; Gómez-Cerezo, M.N.; Kubacka, A.; Fernández-García, M. Boosting Pt/TiO_2 Hydrogen Photoproduction through Zr Doping of the Anatase Structure: A Spectroscopic and Mechanistic Study. *Chem. Eng. J.* **2020**, *398*, 125665. [CrossRef]
29. Pérez-Larios, A.; Rico, J.L.; Anaya-Esparza, L.M.; Vargas, O.A.G.; González-Silva, N.; Gómez, R. Hydrogen Production from Aqueous Methanol Solutions Using Ti–Zr Mixed Oxides as Photocatalysts under UV Irradiation. *Catalysts* **2019**, *9*, 938. [CrossRef]
30. Li, Y.; Xiang, Y.; Peng, S.; Wang, X.; Zhou, L. Modification of Zr-Doped Titania Nanotube Arrays by Urea Pyrolysis for Enhanced Visible-Light Photoelectrochemical H_2 Generation. *Electrochim. Acta* **2013**, *87*, 794–800. [CrossRef]
31. Touam, T.; Atoui, M.; Hadjoub, I.; Chelouche, A.; Boudine, B.; Fischer, A.; Boudrioua, A.; Doghmane, A. Effects of Dip-Coating Speed and Annealing Temperature on Structural, Morphological and Optical Properties of Sol-Gel Nano-Structured TiO_2 Thin Films. *Eur. Phys. J. Appl. Phys.* **2014**, *67*, 30302. [CrossRef]
32. Oh, S.H.; Kim, D.J.; Hahn, S.H.; Kim, E.J. Comparison of Optical and Photocatalytic Properties of TiO_2 Thin Films Prepared by Electron-Beam Evaporation and Sol–Gel Dip-Coating. *Mater. Lett.* **2003**, *57*, 4151–4155. [CrossRef]
33. Ranjitha, A.; Muthukumarasamy, N.; Thambidurai, M.; Balasundaraprabhu, R.; Agilan, S. Effect of Annealing Temperature on Nanocrystalline TiO_2 Thin Films Prepared by Sol–Gel Dip Coating Method. *Optik* **2013**, *124*, 6201–6204. [CrossRef]
34. Johari, N.D.; Rosli, Z.M.; Juoi, J.M.; Yazid, S.A. Comparison on the TiO_2 Crystalline Phases Deposited via Dip and Spin Coating Using Green Sol–Gel Route. *J. Mater. Res. Technol.* **2019**, *8*, 2350–2358. [CrossRef]
35. Teeparthi, S.R.; Awin, E.W.; Kumar, R. Dominating Role of Crystal Structure over Defect Chemistry in Black and White Zirconia on Visible Light Photocatalytic Activity. *Sci. Rep.* **2018**, *8*, 5541. [CrossRef] [PubMed]

36. Shaddad, M.N.; Cardenas-Morcoso, D.; García-Tecedor, M.; Fabregat-Santiago, F.; Bisquert, J.; Al-Mayouf, A.M.; Gimenez, S. TiO_2 Nanotubes for Solar Water Splitting: Vacuum Annealing and Zr Doping Enhance Water Oxidation Kinetics. *ACS Omega* **2019**, *4*, 16095–16102. [CrossRef] [PubMed]
37. Godoy Junior, A.; Pereira, A.; Gomes, M.; Fraga, M.; Pessoa, R.; Leite, D.; Petraconi, G.; Nogueira, A.; Wender, H.; Miyakawa, W.; et al. Black TiO_2 Thin Films Production Using Hollow Cathode Hydrogen Plasma Treatment: Synthesis, Material Characteristics and Photocatalytic Activity. *Catalysts* **2020**, *10*, 282. [CrossRef]
38. Flores-Caballero, A.A.; Manzo-Robledo, A.; Alonso-Vante, N. The Cerium/Boron Insertion Impact in Anatase Nano-Structures on the Photo-Electrochemical and Photocatalytic Response. *Surfaces* **2021**, *4*, 54–65. [CrossRef]
39. Naumenko, A.; Gnatiuk, I.; Smirnova, N.; Eremenko, A. Characterization of Sol–Gel Derived TiO_2/ZrO_2 Films and Powders by Raman Spectroscopy. *Thin Solid Film.* **2012**, *520*, 4541–4546. [CrossRef]
40. Ji, C.H.; Kim, K.T.; Oh, S.Y. High-Detectivity Perovskite-Based Photodetector Using a Zr-Doped TiO_x Cathode Interlayer. *RSC Adv.* **2018**, *8*, 8302–8309. [CrossRef]
41. Bensouici, F.; Bououdina, M.; Dakhel, A.A.; Souier, T.; Tala-Ighil, R.; Toubane, M.; Iratni, A.; Liu, S.; Cai, W. Al Doping Effect on the Morphological, Structural and Photocatalytic Properties of TiO_2 Thin Layers. *Thin Solid Film.* **2016**, *616*, 655–661. [CrossRef]
42. Lee, S.-M.; Joo, Y.-H.; Kim, C.-I. Influences of Film Thickness and Annealing Temperature on Properties of Sol–Gel Derived ZnO–SnO_2 Nanocomposite Thin Film. *Appl. Surf. Sci.* **2014**, *320*, 494–501. [CrossRef]
43. Nakanishi, Y.; Kato, K.; Horikawa, M.; Yonekura, M. Influence of Zn-Sn Ratio on Optical Property and Microstructure of Zn-Sn-O Films Deposited by Magnetron Sputtering. *Thin Solid Film.* **2016**, *612*, 231–236. [CrossRef]
44. Sanchez-Martinez, A.; Koop-Santa, C.; Ceballos-Sanchez, O.; López-Mena, E.R.; González, M.A.; Rangel-Cobián, V.; Orozco-Guareño, E.; García-Guaderrama, M. Study of the Preparation of TiO_2 Powder by Different Synthesis Methods. *Mater. Res. Express* **2019**, *6*, 085085. [CrossRef]
45. Haryński, Ł.; Olejnik, A.; Grochowska, K.; Siuzdak, K. A Facile Method for Tauc Exponent and Corresponding Electronic Transitions Determination in Semiconductors Directly from UV–Vis Spectroscopy Data. *Opt. Mater.* **2022**, *127*, 112205. [CrossRef]
46. Schubert, E.F. *Physical Foundations of Solid-State Devices*, 2022nd ed.; E. Fred Schubert: New York, NY, USA, 2020.
47. Fang, D.; Huang, K.; Liu, S.; Huang, J. Fabrication and Photoluminiscent Properties of Titanium Oxide Nanotube Arrays. *J. Braz. Chem. Soc.* **2008**, *19*, 1059–1064. [CrossRef]
48. Méndez-López, A.; Zelaya-Ángel, O.; Toledano-Ayala, M.; Torres-Pacheco, I.; Pérez-Robles, J.F.; Acosta-Silva, Y.J. The Influence of Annealing Temperature on the Structural and Optical Properties of ZrO_2 Thin Films and How Affects the Hydrophilicity. *Crystals* **2020**, *10*, 454. [CrossRef]
49. Nabi, G.; Raza, W.; Tahir, M.B. Green Synthesis of TiO_2 Nanoparticle Using Cinnamon Powder Extract and the Study of Optical Properties. *J. Inorg. Organomet. Polym. Mater.* **2020**, *30*, 1425–1429. [CrossRef]
50. Komaraiah, D.; Radha, E.; Sivakumar, J.; Ramana Reddy, M.V.; Sayanna, R. Photoluminescence and Photocatalytic Activity of Spin Coated Ag+ Doped Anatase TiO_2 Thin Films. *Opt. Mater.* **2020**, *108*, 110401. [CrossRef]
51. Hou, L.; Zhang, M.; Guan, Z.; Li, Q.; Yang, J. Effect of Annealing Ambience on the Formation of Surface/Bulk Oxygen Vacancies in TiO_2 for Photocatalytic Hydrogen Evolution. *Appl. Surf. Sci.* **2018**, *428*, 640–647. [CrossRef]
52. Goswami, P.; Ganguli, J.N. Tuning the Band Gap of Mesoporous Zr-Doped TiO_2 for Effective Degradation of Pesticide Quinalphos. *Dalton Trans.* **2013**, *42*, 14480. [CrossRef] [PubMed]
53. Tudu, B.; Nalajala, N.; Saikia, P.; Gopinath, C.S. Cu–Ni Bimetal Integrated TiO_2 Thin Film for Enhanced Solar Hydrogen Generation. *Sol. RRL* **2020**, *4*, 1900557. [CrossRef]
54. Cruz, M.R.A.; Sanchez-Martinez, D.; Torres-Martínez, L.M. Optical Properties of TiO_2 Thin Films Deposited by DC Sputtering and Their Photocatalytic Performance in Photoinduced Process. *Int. J. Hydrogen Energy* **2019**, *44*, 20017–20028. [CrossRef]
55. Alfaro Cruz, M.R.; Sanchez-Martinez, D.; Torres-Martínez, L.M. TiO_2 Nanorods Grown by Hydrothermal Method and Their Photocatalytic Activity for Hydrogen Production. *Mater. Lett.* **2019**, *237*, 310–313. [CrossRef]
56. Zdorovets, M.; Kozlovskiy, A.; Tishkevich, D.; Zubar, T.; Trukhanov, A. The Effect of Doping of TiO_2 Thin Films with Low-Energy O^{2+} Ions on Increasing the Efficiency of Hydrogen Evolution in Photocatalytic Reactions of Water Splitting. *J. Mater. Sci. Mater. Electron.* **2020**, *31*, 21142–21153. [CrossRef]
57. Khan, M.A.; Sinatra, L.; Oufi, M.; Bakr, O.M.; Idriss, H. Evidence of Plasmonic Induced Photocatalytic Hydrogen Production on Pd/TiO_2 Upon Deposition on Thin Films of Gold. *Catal. Lett.* **2017**, *147*, 811–820. [CrossRef]
58. Naseri, N.; Kim, H.; Choi, W.; Moshfegh, A.Z. Optimal Ag Concentration for H_2 Production via Ag:TiO_2 Nanocomposite Thin Film Photoanode. *Int. J. Hydrogen Energy* **2012**, *37*, 3056–3065. [CrossRef]
59. Alenzi, N.; Liao, W.-S.; Cremer, P.S.; Sanchez-Torres, V.; Wood, T.K.; Ehlig-Economides, C.; Cheng, Z. Photoelectrochemical Hydrogen Production from Water/Methanol Decomposition Using Ag/TiO_2 Nanocomposite Thin Films. *Int. J. Hydrogen Energy* **2010**, *35*, 11768–11775. [CrossRef]
60. Dholam, R.; Patel, N.; Santini, A.; Miotello, A. Efficient Indium Tin Oxide/Cr-Doped-TiO_2 Multilayer Thin Films for H_2 Production by Photocatalytic Water-Splitting. *Int. J. Hydrogen Energy* **2010**, *35*, 9581–9590. [CrossRef]
61. Liu, E.; Kang, L.; Yang, Y.; Sun, T.; Hu, X.; Zhu, C.; Liu, H.; Wang, Q.; Li, X.; Fan, J. Plasmonic Ag Deposited TiO_2 Nano-Sheet Film for Enhanced Photocatalytic Hydrogen Production by Water Splitting. *Nanotechnology* **2014**, *25*, 165401. [CrossRef]
62. Strataki, N.; Lianos, P. Optimization of Parameters for Hydrogen Production by Photocatalytic Alcohol Reforming in the Presence of Pt/TiO_2 Nanocrystalline Thin Films. *J. Adv. Oxid. Technol.* **2008**, *11*, 111–115. [CrossRef]

63. Dholam, R.; Patel, N.; Adami, M.; Miotello, A. Physically and Chemically Synthesized TiO_2 Composite Thin Films for Hydrogen Production by Photocatalytic Water Splitting. *Int. J. Hydrogen Energy* **2008**, *33*, 6896–6903. [CrossRef]
64. Ibarra-Rodríguez, L.I.; Garay-Rodríguez, L.F.; Hernández-Majalca, B.C.; Domínguez-Arvizu, J.L.; López-Ortiz, A.; Torres-Martínez, L.M.; Collins-Martínez, V.H. N–TiO_2/MO (M: Ni, Cu) Films for Hydrogen Production Using Visible Light. *Int. J. Hydrogen Energy*, 2024; *in press*. [CrossRef]
65. Méndez, F.J.; Barrón-Romero, D.; Pérez, O.; Flores-Cruz, R.D.; Rojas-Challa, Y.; García-Macedo, J.A. A Highly Efficient and Recyclable Pt/TiO_2 Thin Film Photocatalytic System for Sustainable Hydrogen Production. *Mater. Chem. Phys.* **2023**, *305*, 127925. [CrossRef]